Bismuth(III) recovery from hydrochloric acid solutions using Amberlite XAD-7 impregnated with a tetraalkylphosphonium ionic liquid

R. Navarro, P. Ruiz, I. Saucedo, E. Guibal

Bismuth(III) recovery from hydrochloric acid solutions using Amberlite XAD-7 impregnated with a tetraalkylphosphonium ionic liquid

R. Navarro [a,*], P. Ruiz [a], I. Saucedo [a], E. Guibal [b,*]

[a] Universidad de Guanajuato, Departamento de Química. Cerro de la Venada s/n, Pueblito de Rocha, C.P. 36040 Guanajuato, Gto, Mexico
[b] Ecole des mines d'Alès, Centre des Matériaux des Mines d'Alès, 6 avenue de Clavières, F-30319 Alès Cedex, France

A B S T R A C T

An Ionic Liquid (IL) (Cyphos IL 101: tetradecyl(trihexyl)phosphonium chloride was immobilized on Amberlite XAD-7 for preparing extractant impregnated resins (EIRs). The IL content was varied between 59 and 586 mg IL g^{-1} EIR. The EIRs were tested for Bi(III) recovery from (0.01–8 M) HCl solutions. The EIRs were very efficient at extracting Bi(III), the sorption efficiency increased with IL content in the resin, but decreased with HCl concentration. Bi(III) was extracted through an ion exchange mechanism involving the binding of its anionic chloro-complexes to IL phosphonium cation. Sorption isotherms were fitted with the Langmuir equation and they were found to be very favorable with maximum sorption capacities up to 84.3 mg Bi g^{-1} EIR (in 1 M HCl solution using an EIR with 401 mg Li g^{-1} EIR at 20 °C). Temperature slightly influenced Bi(III) sorption capacity. Bi(III) recovery selectivity was studied in bimetallic (1 M HCl) solutions, where, Cu(II) and Ni(II) were not removed but Zn(II) was partially extracted slightly affecting Bi(III) recovery. Sorption kinetics was not affected by agitation speed: the resistance to film diffusion is not the limiting step. The uptake kinetics were controlled by the resistance to intraparticle diffusion. The intraparticle diffusivity coefficients decreased with increasing IL loading but increased with temperature due to the decrease of IL viscosity (in the EIRs). Bi(III) can be easily desorbed from EIRs using either citric acid, nitric acid or sodium sulfate solutions. The EIRs could be recycled maintaining high efficiencies for sorption and desorption for at least five cycles.

Keywords:
Tetraalkylphosphonium ionic liquid
Amberlite XAD-7
Extractant impregnated resin
Bismuth
Sorption

1. Introduction

The regulations concerning the discharge of contaminants in the environment, the strong incentive to recover valuable sub-products (including metal ions) from waste materials, which is sometime called the "urban mine" (including industrial waste materials), have initiated for the last decade an increasing attention to alternative processes for waste valorization. However, there is still a need to develop new processes that could improve the recycling of end-of-life products [1]. Strategic, precious or toxic metals are concerned to face environmental reasons, economic issues or strategic independence criteria. However, the cost of base metals has extended this interest for metal recycling to copper. Waste materials (from electronic materials for example) have become an interesting resource for multi-metal recovery [2]. The valorization of these wastes requires developing processes that allow their selective separation [3]. The valorization of these materials may appeal either pyro-metallurgical or hydrometallurgical processes. In the hydrometallurgical way bismuth is frequently found in the effluents issued from the dismantling of printed circuit boards [2], the purification of copper refinery electrolytes [4], where it is associated with several metals including copper. The acidic leaching of the waste materials and the copper refinery electrolyte could be valorized under the condition to develop selective separation processes. Bismuth can be recovered from water solutions using different mechanisms depending on the composition of the solutions: especially pH but also the presence of competitor ions, high ionic strength etc. Extractants such as Cyanex 301 (and other organophosphoric and organophosphinic acids) were efficiently used for Bi(III) recovery by direct solvent extraction [5,6] or using supported membranes [7]. These solvent extraction processes are preferentially oriented toward the treatment of concentrated solutions. Sorption processes are more appropriate for the recovery of metal ions from dilute solutions. Biosorbents were tested for the recovery of Bi(III), using for example bayberry tannins immobilized on collagen fibers [8], or derivatives of chitosan [9]. Some synthetic resins have been tested for Bi(III) recovery from solutions [10–13]. Mineral sorbents such as

* Corresponding authors. Tel.: +33 (0)466782734; fax: +33 (0)466782701.
E-mail addresses: navarrm@ugto.mx (R. Navarro), Eric.Guibal@mines-ales.fr (E. Guibal).

silica-grafted materials revealed to be promising for recovery of bismuth from dilute (and weakly acidic) effluents [14]. Extractant impregnated resins represent alternative solutions that combine the confinement/immobilization of liquid extractants and their high affinity for metal ions [15]: they are suitable for the treatment of dilute solutions and they retain the selectivity of extractants while avoiding loss of toxic and/or expensive materials (as it may occur in certain cases in solvent extraction processes). A new generation of extractants have been recently developed combining a high efficiency for metal binding, a low vapor pressure and a high solvating effects: ionic liquids (IL, including phosphonium-based or imidazolium-based ILs) have retained a great deal attention for the last decades for extraction processes [16–21]. Hence, phosphonium ionic liquids have been also used as the impregnation phase in different systems including silica materials [22], synthetic polymers [23], resins [24–26] or encapsulated in biopolymers [27–29].

This study focuses on the use of Cyphos IL101 (a phosphonium ionic liquid) for the impregnation of a synthetic resin (Amberlite XAD-7). The extractant-impregnated resin (EIR) has been tested for Bi(III) solutions. SEM–EDX analysis is used for characterizing the materials before and after metal binding. The impact of IL content and HCl concentration have been investigated and the sorption isotherms are established at different IL loadings, and different temperatures. The uptake kinetics are thoroughly investigated with a special attention paid to the resistance to intraparticle diffusion in relation with IL loading and temperature (considering also the effects of metal concentration and agitation speed). The selectivity of the resin for against different metals is investigated from binary solutions (including Zn(II), Ni(II) and Cu(II)). Metal desorption and resin recycling are finally carried out for 5 sorption/desorption cycles.

2. Material and methods

2.1. Materials

Amberlite XAD-7 was supplied by Sigma–Aldrich (Saint-Louis, USA). This is a polyacrylic acid ester type resin ([CH_2–CH(COOR)]n). Amberlite XAD-7 can be considered as a nonionic, moderately hydrophilic macroporous polymer. It is commercialized as a macroporous polymer, although it must be considered as a mesoporous material (pore diameter: 20–500 Å) according to IUPAC. The size range of resin particle was 250–850 μm (20/60 mesh). The specific surface area was 450 $m^2\ g^{-1}$, the porosity was 0.55 and the pore volume was in the range 0.97–1.14 $mL\ g^{-1}$ (skeletal density close to 1.24 $g\ mL^{-1}$) [30]. The resin was conditioned by the supplier with NaCl and Na_2CO_3 to retard bacterial growth. It was necessary to clean it to remove salts and monomeric material present on the resin. The resin was therefore rinsed with de-mineralized water, and then it was put into contact with ketone for 24 h at 25 °C. After filtration under vacuum to remove excess ketone, the resin was rinsed with de-mineralized water. It was then washed with nitric acid (0.1 M) for 24 h. The resin was filtered under vacuum and then rinsed with de-mineralized water to a constant pH. Finally, it was put into contact with ketone for 12 h before being filtered under vacuum and dried in a roto-vapor at 80 °C. Cyphos IL-101 was kindly supplied by Cytec (Canada). This is a phosphonium salt ([P R_3R']$^+$ Cl^-, where R = hexyl and R′ = tetradecyl: tetradecyl(trihexyl) phosphonium chloride, C.A.S. number: 258864-54-9, formula weight: 519 $g\ mol^{-1}$). It is a slightly viscous room temperature ionic liquid. It is less dense than water and looks colorless to pale yellow. It is immiscible with water although it is sparingly soluble in water and can dissolve up to 8% water. Other reagents (metal salts: $BiCl_3$, nickel, copper and zinc nitrate salts, acids…) were analytical grade and supplied by KEM (Mexico). Standard metal solutions were supplied by Perkin Elmer (USA).

2.2. Resin impregnation

In the present work, the extractant was immobilized on the resin by a physical technique. Different processes may be used for the physical impregnation of the resin including (i) the wet method, (ii) the dry method, (iii) the impregnation in the presence of a modifying agent, or (iv) the dynamic method [31]. Previous studies have shown that the dry method increases the stability of the extractant on the resin. The dry impregnation of the resin was actually performed by contacting 5 g of conditioned Amberlite XAD-7 with 25 mL of ketone for 24 h [32]. Varying amounts of Cyphos IL-101, diluted in ketone, were added to the resin slurry for 24 h, under agitation. The solvent was then slowly removed by evaporation in a roto-vapor. The amount of extractant immobilized on the resin (q_{IL}, mg IL g^{-1} EIR) was quantified by the following procedure. A known amount of impregnated resin (250 mg) was mixed with methanol (5 mL) for 24 h to dissolve the extractant, and the solvent was separated from the resin by decantation. The washing treatment was repeated four times. Finally, the resin was dried at 50 °C for 24 h for final evaporation of the solvent. The mass difference ($M_{CyphosIL\text{-}101}$) between impregnated ($M_{XAD\text{-}7/CyphosIL\text{-}101}$) and the washed resin ($M_{XAD\text{-}7}$) was used to calculate the amount of extractant immobilized on the EIR:

$$q_{IL} = \frac{M_{XAD-7/Cyphos\ IL-101} - M_{XAD-7}}{M_{XAD-7/Cyphos\ IL-101}} \quad (1)$$

The experimental procedure allowed the preparation of EIR containing from 59 mg IL g^{-1} EIR up to 586 mg IL g^{-1} EIR.

2.3. Sorption procedures

Bi(III) solutions were prepared in HCl solutions of different concentrations (0.5–6 M) with metal concentrations ranging between 50 and 400 mg Bi L^{-1}. The sorption experiments at equilibrium were performed by mixing the resin with Bi(III) solutions for 24–120 h with a sorbent dosage (SD, solid/liquid ratio) fixed to m/V = 2 g EIR L^{-1} (m: mass of sorbent, V: volume of solution). The suspensions were agitated on a reciprocal shaker (SEV, INO 650V-7) with an agitation speed (v) of 150 movements per minute at constant temperature. After filtration the samples were analyzed by atomic absorption spectrometry (AAS Perkin Elmer AAnalyst 200). The amount of metal adsorbed (q, mg Bi g^{-1} EIR, or mmol Bi g^{-1} EIR) was calculated by the mass balance equation: $q = V(C_0 - C_{eq})/m$, where C_0 and C_{eq} (mg Bi L^{-1}, or mmol Bi L^{-1}) are the initial and equilibrium Bi(III) concentrations, respectively. Several sorption kinetic experiments were performed by contact under agitation of a fixed amount of EIR (1 g of resin loaded with IL in the range 207–586 mg extractant g^{-1} EIR) with a fixed volume (500 mL; SD: 2 g EIR L^{-1}) of 1 M HCl solution containing varying concentrations (in the range 150–500 mg Bi(III) L^{-1}). The sorption took place in a closed jacketed tank reactor under mechanical agitation (Shaker IKA, RW-20, at 150 or 250 rpm). The spaces available around the axis of the stirrer and for sampling were small enough to prevent water evaporation and temperature variation. Temperature (T) was varied in the range 10–40 °C. The samples were collected at fixed times by a syringe connected to a filtration grid and residual bismuth concentrations were determined by AAS. After analysis, the samples were returned to the reactor in order to avoid variation in solution volume.

Modeling of sorption isotherms and uptake kinetics are described in the Additional Material Section (together with some examples of modeling, Fig. AM1).

2.4. Desorption and recycling procedures

For the study of Bi(III) desorption, 20 mg of EIR (extractant loading: 401 mg extractant g^{-1} EIR) was mixed with 10 mL of Bi(III) solution (100 mg Bi(III) L^{-1} in 1 M HCl solution) for 24 h. The residual concentration measured by AAS after filtration served to determine the amount of metal bound to the resin. The metal-loaded resin was mixed for 24 h with 10 mL of eluent solution (including KI (0.25 M in 0.1 M HCl), Na_2SO_4 (0.5 M, pH 2), EDTA (0.05 M, pH 6), citric acid (0.05 M, pH 6) and nitric acid (2 M)). The desorption step was repeated once (when necessary). After filtration, the concentration in the eluent was determined by AAS in order to obtain the amount of Bi desorbed from the resin. The amount of metal desorbed divided by the amount of metal bound to the EIR served for calculating the desorption yield (or efficiency). Washing steps were performed under agitation for 2 h after metal sorption (using 10 mL of demineralized water) and after metal desorption (using 10 mL of 1 M HCl solution, washing step being repeated one time). Bi(III) in the washing phase was analyzed to evaluate the necessity of these washing steps. For the evaluation of sorption/desorption cycles, the same procedure was used for five successive cycles.

2.5. SEM and SEM–EDX analyses

An environmental scanning electron microscope (ESEM), Quanta FEG 200, coupled with an Oxford INCA350 energy dispersive X-ray microanalysis (EDX) system was used for SEM–EDX characterization of materials before and after metal sorption. The system can be used to acquire qualitative or quantitative spot analyses and qualitative or quantitative X-ray elemental maps and line scans. This ESEM allows samples to be analyzed at pressure and humidity which approach normal laboratory conditions and avoids experimental artifact. More specifically, this is possible to analyze the samples at much higher pressures than with conventional SEM. For cross-section analysis, the resin particles were frozen in liquid nitrogen prior to a mechanical breaking in order to obtain observable cross-sections.

3. Results and discussion

3.1. Characterization of EIRs

3.1.1. IL loading

The impregnation of Amberlite XAD-7 with Cyphos IL101 was extensively described in a previous study on the synthesis of Cd sorbent [24]. Different lots were prepared with IL loading varying between 59 and 586 mg IL g^{-1} EIR. The impregnation procedure allowed complete retention of the IL till the limit amount of 15 g of IL (diluted in ketone) for 10 g of Amberlite XAD-7: the amount of IL released from EIR after ethanol washing corresponded to the amount of IL introduced in the impregnation bath. Above, IL release imparted the possible use of the EIR for metal sorption. The EIRs were analyzed by optical microscopy [24]. Amberlite XAD-7 aspect changed with increasing IL loading: the resin particles progressively became more opaque up to 500 mg IL g^{-1} EIR, above the resins became translucent due to light diffraction effects at the surface of the resin particles fully covered by the IL: the porous network of the resin being saturated. The textural study of EIRs revealed that the pore diameter increased with IL loading (from 84 Å for Amberlite XAD-7 to 434 Å for EIRs with a 498 mg IL g^{-1} EIR load) [24]: the porous network was progressively filled beginning with micropores, and following with mesopores. As a consequence the specific surface area of EIRs strongly decreased from 499 $m^2\ g^{-1}$ for Amberlite XAD-7 to 22 $m^2\ g^{-1}$ for high IL loaded resins (498 mg IL g^{-1} EIR). SEM–EDX analysis of EIRs also showed that the IL (traced by the P element) was homogeneously distributed in the whole mass of the sorbent.

3.1.2. SEM–EDX analysis of Bi(III)-loaded EIR

The Bi(III) sorption on the EIR was characterized using SEM–EDX analysis. Fig. 1 shows (a) the cross-section of the EIR after Bi(III) sorption, (b) the X-ray spectrum (identifying the main elements present on the section; i.e., C and O elements that trace Amberlite XAD-7 core; P element that traces the IL; and Bi element; C element can come from both the IL and bound metal, under the form of chloro-complex), and (c) the cartography of main elements. The cross-section is characterized by the presence of an homogeneous and dense dispersion of small dots at the periphery of the resin particle (first external 20 μm) and the presence of a scarce (but homogeneous) distribution of largest dots in the core of the particle. The cartography of main elements clearly shows the homogeneous distribution of C/O elements (for the resin structure), P element (for IL) and Bi element (for solute): this confirms that both the IL and the metal are equally distributed in the whole mass of the sorbent. This is confirmed by Fig. AM2 (see Additional material Section) that shows the distribution of the elements along the cross-section of the cut particle (following white line): the distribution profile is homogeneous for all elements. The P and Bi (together with Cl) elements are correlated confirming that the metal binding occurs directly by interaction with the IL. Fig. AM3 (See Additional Material Section) compares the X-ray spectra of "white spots" (called Spectre 1) and "mass zone" of the resin particle (called Spectre 2). Though the "analytical pear" is not selective enough for analyzing only the white spot (analysis of a given volume around the spot, including the first internal layers of the resin) the inversion in the intensity of Bi and P elements (white spot: Bi $\gg$ P; mass zone: P > Bi) clearly shows that some heterogeneities exist at the microscopic scale. White spots are enriched in Bi compared to other zones of the Bi(III)-loaded EIR: this is probably due to the aggregation of Bi nanoparticles as the result of possible localized precipitation phenomena.

3.2. Influence of HCl concentration and IL loading on Bi(III) sorption efficiency

Fig. 2 describes the cross effects of HCl concentration (0.5–6 M) and IL loading (q_{IL}: 0–586 mg IL g^{-1} EIR) on Bi(III) sorption efficiency (Fig. 2A) and on the distribution coefficient (D: $[Bi]_{EIR}$/[Bi]solution, at equilibrium, L kg^{-1}; Fig. 2B). Amberlite XAD-7 cannot bind Bi(III) whatever the concentration of HCl: this contrasts with other systems that showed that, especially at high HCl concentration, the partial oxidation of some reactive groups at the surface of the resin (conversion of polyacrylic acid ester groups to carboxylic acid groups) can bind small amounts of metal ions such as chloro-anions of Au(III) [33], or Cd(II) [24]. As expected, increasing the IL load in the EIR progressively and linearly increased the sorption efficiency of the EIR, especially at low HCl concentration.

On the other hand the concentration of HCl strongly influenced Bi(III) recovery. For low IL loading (0–207 mg IL g^{-1} EIR) the sorption efficiency progressively decreased when increasing HCl concentration. For higher IL loading three HCl concentration ranges can be identified: (a) for 0.5–2 M HCl solutions the sorption efficiency hardly varied, (b) for 2–4 M HCl solutions the sorption efficiency slightly decreased, and (c) for HCl concentration above 4 M Bi(III) sorption efficiency more significantly decreased.

The curves can be analyzed taking into account Bi(III) speciation in HCl solutions. Fig. AM4 (See Additional Material Section) shows the distribution of the different chloro-species of Bi(III) in function of chloride ions concentration (which in turn corresponds to HCl concentration). The species distribution diagram was established using the overall formation constants of Bi(III) chlorocomplexes

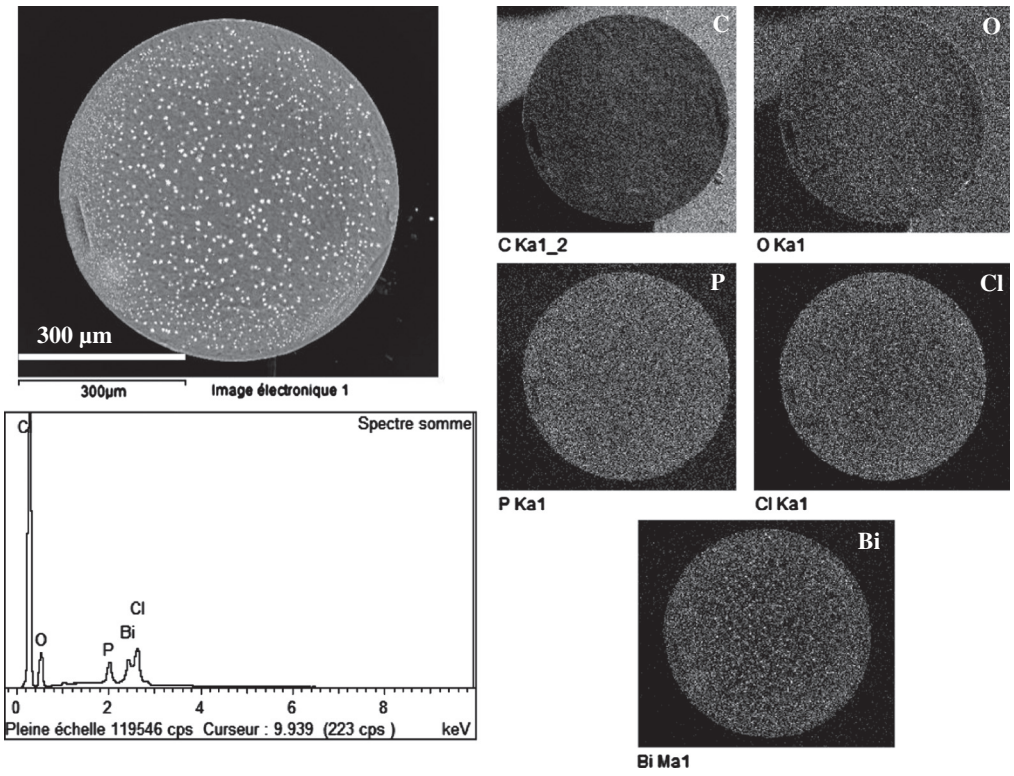

Fig. 1. IL-impregnated Amberlite XAD-7 after Bi(III) sorption: cross-section view, cartography of elements (C, O, P, Cl and Bi) and X-ray pattern.

($BiCl_i^{3-i}$) cited by Högfeldt: log βi = 2.53, 4.66, 6.32, 7.93, 8.18, and 6.00, for i = 1–6, respectively [34]. Grey-shaded zone represents the HCl concentration range that was investigated in this study (0.5–6.0 M). Bi(III) can form, in the presence of chloride ions a series of different chloro-complexes, including: (a) Cationic complexes: $BiCl^{2+}$, $BiCl_2^+$, (b) Neutral complexes: $BiCl_3$, and (c) Anionic complexes: $BiCl_4^-$, $BiCl_5^{2-}$, $BiCl_6^{3-}$. As the concentration of chloride ions (and HCl) increases the speciation of Bi(III) changes toward the formation of more anionic species. In the range of HCl concentrations that was studied in the present work the anionic species represent more than 95% of total Bi(III). Cyphos IL101 is a tetraalkylphosphonium IL that can be schematized under the form $R^3R'P^+Cl^-$. Previous studies have shown the affinity of the cationic phosphonium moiety for anionic species [17,30,33,35]; through ion exchange with chloride ions (counter anion of the IL). Bismuth recovery from HCl solution will thus proceed through different possible reactions:

$$BiCl_4^- + R_3R'P^+Cl^- \leftrightarrow R_3R'P^+BiCl_4^- + Cl^- \quad (2)$$

$$BiCl_5^{2-} + 2R_3R'P^+Cl^- \leftrightarrow (R_3R'P^+)_2BiCl_5^{2-} + 2Cl^- \quad (3)$$

$$BiCl_6^{3-} + 3R_3R'P^+Cl^- \leftrightarrow (R_3R'P^+)_3BiCl_6^{3-} + 3Cl^- \quad (4)$$

The decrease in sorption efficiency at high HCl concentration can be explained by the effect of large chloride ions excess that contributes to the dissociation of the $(R_3R'P^+)_i\ BiCl_{3+i}^{i-}$ complexes. Since the predominating species are the mono and di-anionic chloro-complexes and the reversal effect less extended for these two species the extraction mechanism will probably involve the extraction of one (or both) of them by Cyphos IL101 immobilized in the porous structure of Amberlite XAD-7.

The log–log plot of the distribution coefficient D vs. q_{IL} and a_{HCl} can be used to determine the stoichiometric ratio between the metal and the extractant, and between the metal and chloride ions, respectively. The slope of the plot allows identifying the number of phosphonium cations and chloride ions that were exchanged. Here, a_{HCl} is the mean activity of H^+ and Cl^- ions and can be used for estimating the chloride ion activity in order to determine the number of chloride ions that are involved in metal sorption (taking into account the impact of ionic strength). The plot of D vs. q_{IL} (in log–log units; Fig. 2B) at all HCl concentration values systematically shows two linear sections with approximately the similar slopes and with a common demarcation at q_{IL} = 207 mg IL g^{-1} EIR. At low IL loading the slope of the logarithmic plot of D vs. q_{IL} was 1.51 ± 0.17 while it increased to 2.54 ± 0.14 at higher IL loading. Based on Eqs. (2)–(4) the slope was expected to be close to 1 (sorption of $BiCl_4^-$), 2 (sorption of $BiCl_5^{2-}$) or 3 (sorption of $BiCl_6^{3-}$). Moreover, the values of slopes for the plots log D vs. log a_{HCl} (not shown) are closed to −0.5. Actually the values of slopes are not consistent with the stoichiometric coefficients on Eqs. (2)–(4). The interpretation of phenomena is made complex because Cyphos IL101 can extract significant amounts of water and HCl [36]. The discussion of slopes (and stoichiometric ratios) is thus difficult.

3.3. Bi(III) sorption isotherms

Sorption isotherms for Bi(III) using Cyphos IL101 immobilized in Amberlite XAD-7 were obtained from 1 M HCl solutions at different temperatures (20–40 °C, Fig. 3) and different IL loadings (106–401 mg IL g^{-1} EIR, Fig. 4). The shape of the curves was systematically characterized by a sharp initial increase of sorption capacity followed by a saturation plateau. This is the typical shape of Langmuir-type sorption isotherm. Actually, the Langmuir equation roughly fitted experimental data: some discrepancies could be observed in the curved part of the isotherms.

3.3.1. Effect of temperature on sorption isotherms

The temperature had a limited impact on sorption isotherms: the sorption capacities slightly increased with temperature,

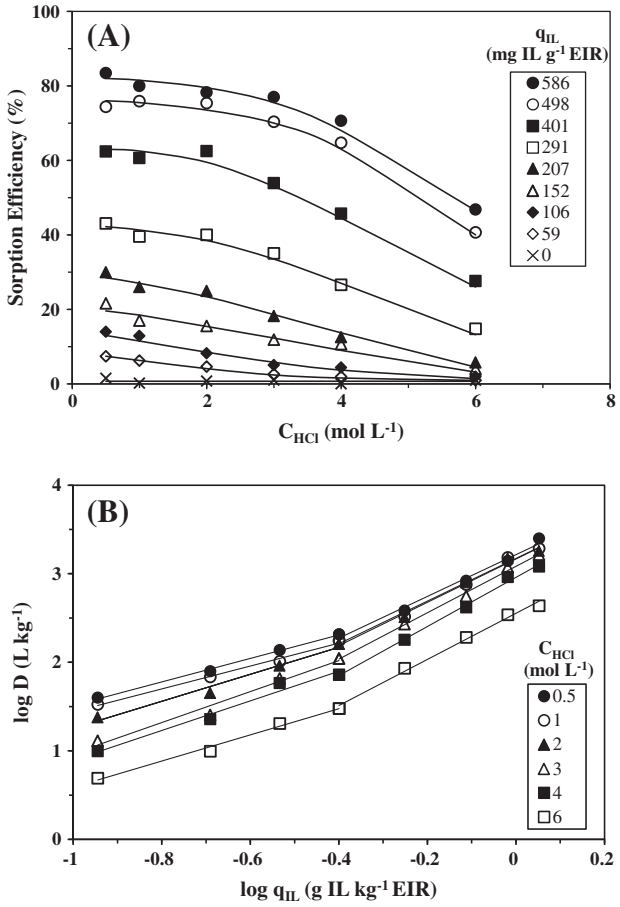

Fig. 2. Effects of HCl concentration and IL loading in the EIR on Bi(III) sorption efficiency (A) and distribution coefficient D (B) (sorbent dosage, SD: 2 g EIR L^{-1}; C_0: 300 mg Bi L^{-1}; T: 20 °C; v: 150 rpm; contact time: 120 h).

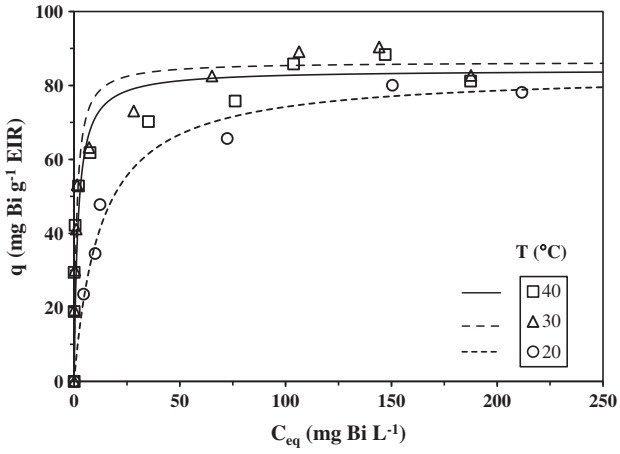

Fig. 3. Effect of temperature on Bi(III) sorption isotherm using IL-impregnated resin (C_{HCl}: 1 M; SD: 2 g EIR L^{-1}; q_{IL}: 401 mg IL g^{-1} EIR; v: 150 rpm; contact time: 120 h).

indicating that the reaction is endothermic. However, the effect could only be detected for the shift 20 °C to 30 °C, above (i.e., at 40 °C) the sorption isotherms overlapped both in terms of maximum sorption capacity and initial slope, which is correlated to the affinity of the sorbent for Bi(III) (Fig. 3). The variations for the coefficients of the Langmuir equation (Table 1) are not showing clear and continuous trends. The sorption capacity at saturation of the monolayer (i.e., q_m) only varied in the range

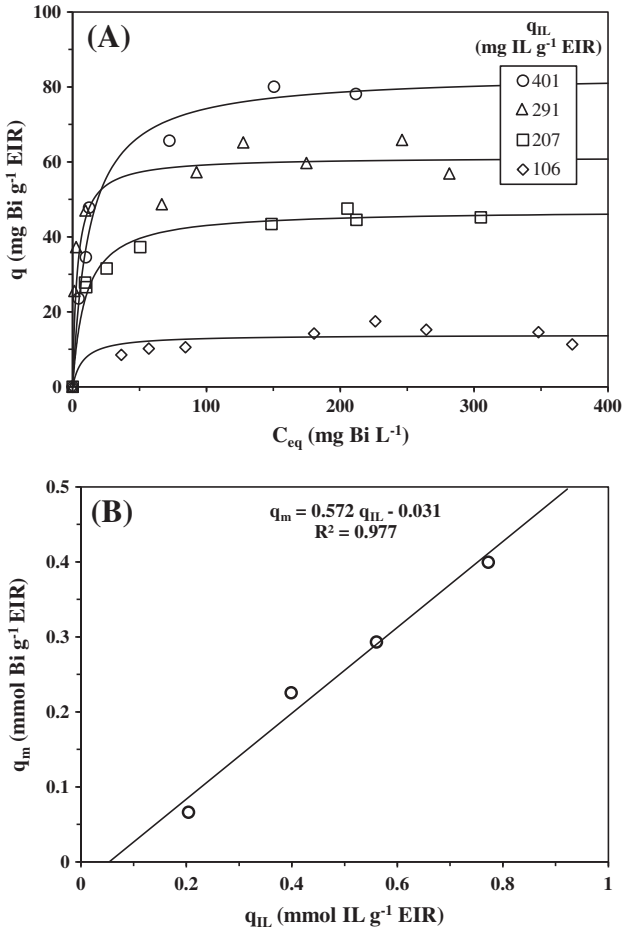

Fig. 4. Effect of IL loading on B(III) sorption isotherm (A) and correlation between IL loading and Bi(III) maximum sorption capacity (B) using IL-impregnated resin (C_{HCl}: 1 M; SD: 2 g EIR L^{-1}; T: 20 °C; v: 150 rpm; contact time: 120 h).

Table 1
Effect of IL loading and temperature on sorption isotherms – parameters of the Langmuir equation. (C_{HCl}: 1 M; SD: 2 g EIR L^{-1}; v: 150 rpm; contact time: 120 h).

IL loading (mg IL g^{-1} EIR)	T (°C)	q_m (mg Bi g^{-1} EIR)	b (L mg^{-1})	R^2	Bi(III)/IL (mol/mol)
106	20	13.9	0.128	0.912	0.32
207	20	47.1	0.104	0.998	0.57
291	20	61.3	0.283	0.988	0.52
401	20	83.5	0.080	0.997	0.52
401	30	86.4	0.835	0.996	0.54
401	40	84.2	0.551	0.995	0.52

83.5–86.4 mg Bi g^{-1} EIR. The affinity coefficient (i.e., b) shows much larger variations especially between 20 °C and 30–40 °C: the difference reaches one order of magnitude between 20 °C and 30 °C. This is a clear evidence that the sorbent has a greater affinity for Bi(III) at higher temperatures. The variations of the parameter are not clear enough to make possible the calculation of thermodynamic parameters.

3.3.2. Effect of IL loading on sorption isotherms

As expected, increasing IL loading in the EIR increased sorption capacities (Fig. 4A). Table 1 shows the increase of sorption capacity at monolayer saturation (i.e., q_m). The plot of q_m vs. q_{IL} (in molar units) follows a linear trend (Fig. 4B). The slope of the curve is close to 0.57; this is consistent with the molar ratio Bi(III)/IL calculated

in Table 1 on the basis of sorption capacities at monolayer saturation and IL content in the EIR. Except for the lowest IL loading (which decreased to 0.32) the molar ratio Bi(III)/IL at saturation varied between 0.52 and 0.57: average value: 0.534; standard deviation: 0.020. A molar ratio close to 0.5 is consistent with the hypothesis of a reaction involving 2 IL molecules per bismuth molecule. This means that the interaction probably proceeds through the interaction between 2 $R_3R'P^+$ Cl^- and $BiCl_5^{2-}$, according Eq. (3). Fig. 4B also shows that the linearization does not pass through the origin. This phenomenon also occurred in the case of Cd(II) sorption in HCl using the same EIRs [24]. This was attributed to the tight binding of a thin layer of IL at the surface of the internal porosity of Amberlite XAD-7: this fraction is supposed to have a strong interaction with the support that imparts its ability to interact with metal ions. A similar mechanism could occur in the case of Bi(III) sorption on Cyphos IL101/Amberlite XAD-7 EIR and this could explain that at low IL loading (i.e., 106 mg IL g^{-1} EIR) the molar ratio Bi(III)/IL did not respect the expected molar ratio (0.32 instead of 0.5). Based on the linear plot of q_m vs. q_{IL} (in molar units) the amount of inactive IL that could be bound to the support may reach up to 0.054 mmol IL g^{-1} EIR (i.e., 28 mg IL g^{-1} EIR). This is consistent with the values calculated in the case of Pd(II) sorption using the same EIRs (i.e., 0.04 and 0.07 mmol IL g^{-1} EIR, depending on the concentration of HCl solutions) [25]. For the low IL loading (i.e., 106 mg IL g^{-1} EIR or 0.204 mmol IL g^{-1} EIR) correcting the IL loading with the fraction of IL tightly bound to the support would result in recalculating the Bi(III)/IL molar ratio to 0.44 closer to the expected value (i.e., 0.5).

The stoichiometric ratio Bi(III)/IL close to 0.5 is consistent with previous results using the same EIRs for Cd(II) sorption ($(R_3R'P^+)_2$ $CdCl_4^{2-}$) [24], for Pd(II) sorption ($(R_3R'P^+)_2$ $PdCl_4^{2-}$) [25] and Zn(II) sorption ($(R_3R'P^+)_2$ $ZnCl_4^{2-}$) [30], while the stoichiometric ratio was close to 1 for Au(III) sorption ($(R_3R'P^+)$ $AuCl_4^-$) [33]. In the case of Bi(III) sorption on Cyphos IL101 immobilized in alginate capsules, Campos et al. observed that the stoichiometric ratio exceeded 1 between the IL and Bi(III) (i.e., in the range 1.3–1.6): they suggested that metal binding involved the reaction ($(R_3R'P^+)$ $BiCl_4^-$) with a number of IL molecules not being available or accessible to metal ions [27].

The comparison of sorption capacities for Bi(III) for different supports is made difficult by the difference in pH or acid concentrations that were investigated. Belkhouche and Didi [15] reported maximum sorption capacities as high as 490 mg Bi g^{-1} EIR at pH 3–4 for di(2-ethylhexyl)phosphoric acid (D2EHPA) impregnated on Amberlite XAD-1180. In the case of Cyphos IL101/Alginate capsules the maximum sorption capacity reached up to 150 mg Bi g^{-1} sorbent in 1 M HCl solutions [27]. Bismuth sorption at pH 2 on coconut activated carbon reached 55 mg Bi g^{-1} [37].

3.4. Influence of metal cations on Bi(III) sorption efficiency – selectivity

The presence of other metals may interfere on the sorption of target metal. This is representative of most common types of effluents where competitor metals may be present in complex solutions. In order to verify the selectivity of the EIR for Bi(III) a series of experiments was performed in binary solutions containing increasing concentrations of competitor metals (100, 200 and 400 mg metal L^{-1} vs. 100 mg Bi L^{-1}), including Cu(II), Ni(II), and Zn(II). Fig. 5 shows the influence of these metal ions on Bi(III) sorption efficiency. The metals can be classified in two groups: (a) Cu(II) and Ni(II) (whose even in large excess hardly affected Bi(III) sorption capacity, less than 2%), and (b) Zn(II) (which weakly decreased Bi(III) sorption capacity). The presence of Zn(II) even with a 12-fold excess (in molar units) compared to Bi(III) reduced the sorption efficiency by less than 10%. The difference in the competitive behavior of these metals can be correlated to their

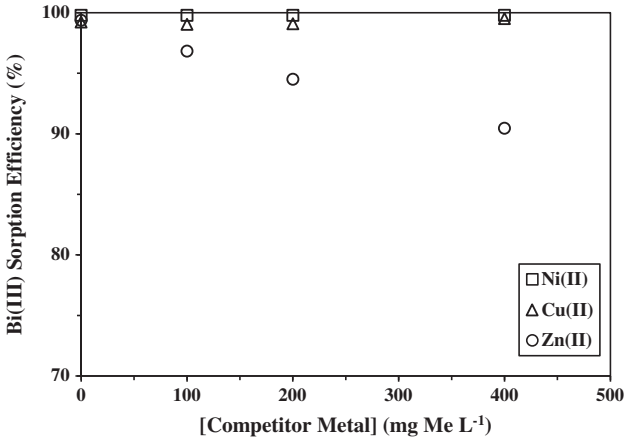

Fig. 5. Effect of the presence of competitor metal ions (Ni(II), Cu(II) and Zn(II)) on Bi(III) sorption efficiency using IL-impregnated resin (C_{HCl}: 1 M; C_0: 100 mg Bi L^{-1}; SD: 2 g EIR L^{-1}; q_{IL}: 401 mg IL g^{-1} EIR; T: 20 °C; v: 150 rpm; contact time: 120 h).

speciation properties in HCl solutions. Indeed, Cu(II) and Ni(II) do not form stable anionic chloro-complexes, contrary to Zn(II) that can form chloro-anionic complexes: $ZnCl_4^{2-}$ and $ZnCl_3^-$. As a matter of fact, Cyphos IL101 was carried out for the solvent extraction of Zn(II) from chloride-containing synthetic and industrial solutions [20,38,39]. Zn(II) was also recovered from HCl solutions (optimum concentration range 2–4 M) using Cyphos IL101/Amberlite XAD-7 EIR: maximum sorption capacity reached 20 mg Zn g^{-1} EIR [30]. Similar results were observed in the sorption of different metals ions using Cyphos IL101 immobilized on Amberlite XAD-7 or in alginate capsules: the sorption of Pd(II) [40], Pt(IV) [29], or Au(III) [35] was weakly affected by the presence of Zn(II) or Fe(III) and almost not influenced by the presence of Ni(II) and Cu(II). The effect of the matrix on target metal sorption can thus be roughly predicted based on the stability of chloro-anionic complexes of the competitor metal ions.

3.5. Bi(III) uptake kinetics

In order to identify the limiting step in the uptake kinetics of Bi(III) by the Cyphos IL101/Amberlite XAD-7 several equations (see Eqs. (AM2)–(AM9) in Additional Material Section) were tested for fitting experimental data. Fig. AM1 (See Additional Material Section) shows an example of model testing (i.e., HDM and SCM affected by film diffusion (FD), intraparticle diffusion (PD) or chemical rate (CR)). The best results were obtained with HDM-PD and to a lesser extent with SCM-PD and SCM-FD (in these cases the linear section was obtained but the fitted curves did not pass through the origin. This is the first evidence that the resistance to intraparticle diffusion is probably the main controlling step in the uptake kinetics. In addition, the pseudo-first order rate equation (PFORE) and the pseudo-second order rate equation (PSORE) failed to accurately fit experimental data: the PSORE failed to fit the curvature zone while the PFORE significantly overestimated the last part of the uptake kinetics (Fig. AM1, See Additional Material Section). For these reasons the uptake kinetics have been modeled using the model of resistance to intraparticle diffusion (the so-called Crank's equation) (see below the fit of experimental curves: solid lines superimposing to experimental dots).

3.5.1. Effect of agitation speed

The increase of agitation speed from 150 rpm to 250 rpm did not significantly affect the kinetic profiles: the curves superimposed (Fig. AM5, See Additional Material Section). This is confirmed by the value of the intraparticle diffusion coefficient

Table 2
Uptake kinetics – intraparticle diffusion coefficient (Crank's equation). (C_{HCl}: 1 M; SD: 2 g EIR L^{-1}; v: 150 rpm).

v (rpm)	q_{IL} (mg IL g^{-1} EIR)	C_0 (mg Bi L^{-1})	T (°C)	$D_e \times 10^{11}$ (m^2 min^{-1})	MSR
150	401	250	20	2.75	0.018
250	401	250	20	3.54	0.006
150	207	250	20	35.2	0.068
150	586	250	20	0.54	0.054
150	401	150	20	1.85	0.015
150	401	500	20	8.53	0.083
150	401	250	10	1.36	0.099
150	401	250	30	6.56	0.015
150	401	250	40	14.4	0.073

MSR: minimum square of residuals.

(i.e., D_e) that hardly varies around 3×10^{-11} m^2 min^{-1} (Table 2). The limited effect of agitation speed confirms that the resistance to film diffusion is not the predominant controlling step. This also justifies the modeling of experimental data with the Crank's equation (resistance to intraparticle diffusion): the experimental points are well described by Eq. (8).

3.5.2. Effect of IL loading in the EIR

The kinetic profiles have been compared under identical conditions using EIRs that contain different IL loadings (Fig. 6A and B). As expected increasing the IL loading contributed to a drastic reduction of the residual concentration at equilibrium. More interesting is the impact of this parameter on the initial section of the curve. When the IL loading increases the initial slope of the curve tends to decrease and the time required for reaching the equilibrium dramatically increases. This is confirmed by the drastic decrease in the intraparticle diffusion coefficient from 35.2×10^{-11} to 0.54×10^{-11} m^2 min^{-1}. With similar material Arias et al. [24] reported that when increasing the loading of the EIR, the IL progressively fills the porous network: in a first step the micropores are filled with the ionic liquid before filling the mesopores (and even macropores when the EIR is saturated). The diffusion of solute is hindered in the IL (compared to water). This limitation can proceed through different mechanisms including viscosity effect: the IL has a greater viscosity than water. For example Alguacil et al. [41] showed that the apparent diffusion coefficient of Cr(VI) in the organic phase (made of Cyphos IL101 and cumene) of a pseudo-emulsion membrane is about one order of magnitude lower than the self-diffusion coefficient of Cr(VI) in water. As a consequence the resistance to intraparticle diffusion increases with the progressive saturation of the internal porous network of the EIR (Table 2). The direct correlation of diffusion coefficient with viscosity is made difficult by the impact of water and HCl extraction by the IL. Indeed, while the water content in the IL increases its viscosity tends to significantly decrease. This means that the diffusivity coefficient in the organic phase will vary along the sorption process with the simultaneous extraction of water and HCl. All these facts contribute to explain the significant contribution of intraparticle diffusion in the control of uptake kinetics.

The intraparticle diffusion coefficients for Bi(III) in Amberlite XAD-7/Cyphos IL101 EIR can be compared to the values obtained with the values obtained with Cyphos IL101 immobilized in alginate capsules [27]. Though the experimental conditions (IL loading, metal concentration) are different the diffusion coefficients are in the same orders of magnitude: 6×10^{-11} m^2 min^{-1}–14.3×10^{-11} m^2 min^{-1} (for alginate encapsulated materials with IL varying between 314 and 573 mg IL g^{-1} sorbent) vs. 5.4×10^{-12} m^2 min^{-1}–3.52×10^{-10} m^2 min^{-1} (for the present system with IL varying between 207 and 586 mg IL g^{-1} EIR). Surprisingly, in the case of alginate-based material the variation in the diffusion coefficient

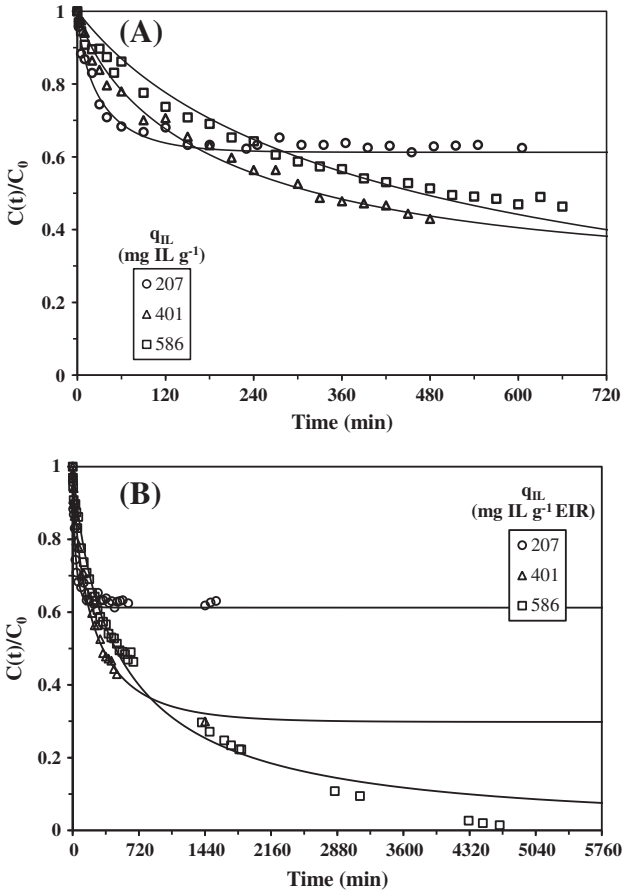

Fig. 6. Effect of IL loading on Bi(III) uptake kinetics using IL-impregnated resin at: (A) the initial stage, and (B) the later stage of process (C_{HCl}: 1 M; C_0: 250 mg Bi L^{-1}; SD: 2 g EIR L^{-1}; T: 20 °C; v: 150 rpm).

was less marked and did not show a continuous trend as it occurred with Amberlite XAD-7 supported IL. It is noteworthy that in alginate-based materials the IL is immobilized in the core of the gel-like structure compared to the present system. The decreasing effect of IL loading increase on diffusion coefficient was also observed for the sorption of Au(III) [33] (5.2×10^{-11} m^2 min^{-1}–16.6×10^{-11} m^2 min^{-1}), Pd(II) [25] (1.6×10^{-11} m^2 min^{-1}–10.5×10^{-11} m^2 min^{-1}), Zn(II) [30] (1.2×10^{-11} m^2 min^{-1}–5.8×10^{-11} m^2 min^{-1}), and Cd(II) [24] (1×10^{-12} m^2 min^{-1}–8×10^{-10} m^2 min^{-1}): the differences being especially marked for Bi(III) and Cd(II).

3.5.3. Effect of metal concentration

The change in the initial metal concentration affects the time required to reach equilibrium while the initial slope was almost not affected (Fig. 7). The concentration gradient is the driving force for mass transfer: increasing the concentration of the metal increase the intraparticle diffusion coefficient. Actually, D_e linearly varied with the equilibrium concentration according to: D_e (m^2 min^{-1}) = $1.25 \times 10^{-11} + 2.34 \times 10^{-13}$ C_{eq} (mg Bi L^{-1}) (R^2: 0.997). Due to the limited number of data, this equation should be considered a simple indication on the trend followed by intraparticle diffusion coefficient against metal concentration effect. In the case of Bi(III) sorption on Cyphos IL101/alginate capsules, Campos et al. [27] also observed an increase of intraparticle diffusion coefficient with metal concentration. Similar variation in the apparent intraparticle diffusion coefficient were observed when increasing

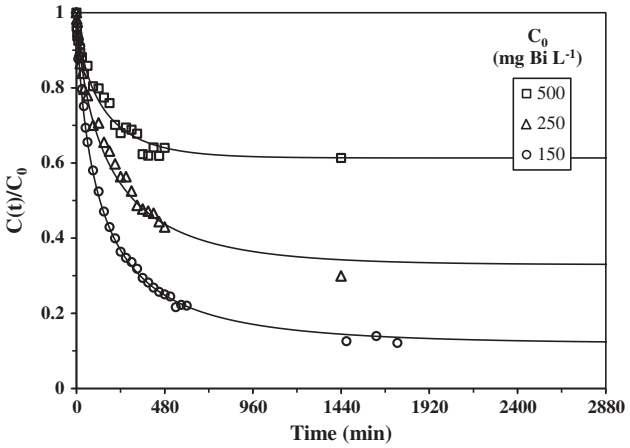

Fig. 7. Effect of initial metal concentration on Bi(III) uptake kinetics using IL-impregnated resin (C_{HCl}: 1 M; q_{IL}: 401 IL g^{-1} EIR; SD: 2 g EIR L^{-1}; T: 20 °C; v: 150 rpm).

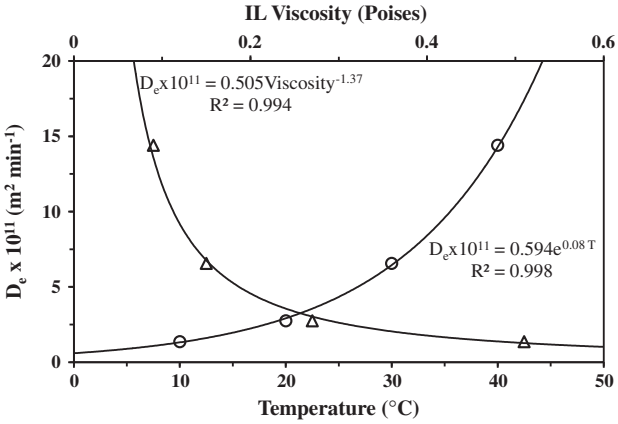

Fig. 9. Correlation of effective diffusion coefficient with temperature (○) and IL viscosity (Δ) (C_{HCl}: 1 M; q_{IL}: 401 mg IL g^{-1} EIR; SD: 2 g EIR L^{-1}; C_0: 250 mg Bi L^{-1}; v: 150 rpm).

metal concentration for the sorption of Au(III), Zn(II), Cd(II) or Pd(II) with the same EIR [24,25,30,33].

3.5.4. Effect of temperature

The temperature frequently affects the thermodynamics of sorption process, though Fig. 6 showed a limited impact of increasing temperature from 20 to 40 °C. However, this parameter can also influence the uptake kinetics. Fig. 8 shows that the temperature significantly changed the kinetic profile both at the initial stage of the process (within the first hours of contact) and at the later stage. More specifically, the initial slope of the uptake kinetics increased with increasing the temperature (Fig. 8A). This can be probably correlated to the effect of temperature on the viscosity of the IL within the porous network. Indeed, according the data sheet of Cytec for Cyphos IL 101, the viscosity of IL varied from 0.51 Poise to 0.09 Poise (values for Cyphos IL101 containing about 10% of water, close to saturation, about two orders of magnitude greater for a 1% w/w water content) when increasing the temperature from 10 to 40 °C. Fig. 9 correlates the effective diffusion coefficient (i.e., D_e) with the temperature (exponential function) and with the viscosity (power function; assuming the IL to be water saturated at 10%). While decreasing the viscosity the mobility of metal ions species is improved and the resistance to intraparticle diffusion decreases. The effect of temperature on viscosity, which in turn affects intraparticle diffusion coefficient (Table 2), is thus consistent with the conclusions reached on the effect of IL loading (see above).

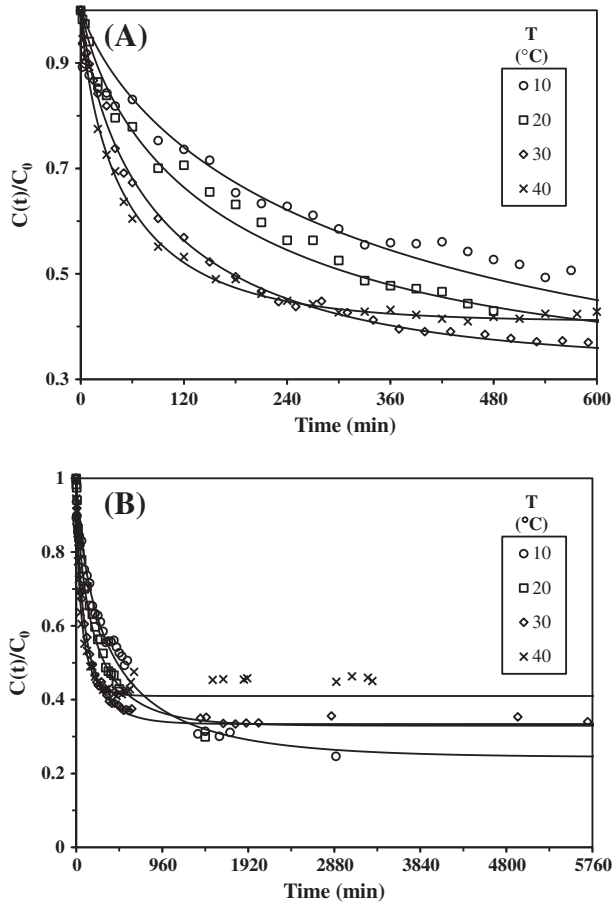

Fig. 8. Effect of temperature on Bi(III) uptake kinetics of IL-impregnated resins at: (A) the initial stage, and (B) the later stage of process (C_{HCl}: 1 M; q_{IL}: 401 mg IL g^{-1} EIR; SD: 2 g EIR L^{-1}; C_0: 250 mg Bi L^{-1}; v: 150 rpm).

3.6. Metal desorption and EIR recycling

The possibility to desorb the target metal and the ability of the EIR to be recycled are key parameters for the development and the transfer of the process for large-scale applications. A series of eluents have been tested for five sorption/desorption cycles including: (a) KI (0.25 M in 0.1 M HCl), EDTA (0.05 M, pH 6) and Na_2SO_4 (0.5 M, pH 2) (their sorption and desorption performances did not follow a clear trend; irregular sorption and desorption efficiencies, progressive decrease of efficiency, necessity to perform at least two successive desorption step before sorption, not shown), and (b) citric acid (0.05 M, pH 6) and nitric acid (2 M) (whose sorption/desorption properties were maintained at high level over the 5 cycles) (Fig. 10). Both nitric acid and citric acid solutions have sorption efficiency almost constant; two successive desorption steps were necessary to completely remove Bi(III): however, the amount released at the second desorption steps was slightly higher for nitric acid than for citric acid. The mass balance performed on Bi(III) over the five cycles showed that with nitric acid the overall desorption efficiency approached 95% while with citric acid the overall desorption (cumulative sorption and desorption) exceeded 99%. Citric acid (0.05 M, pH 6) achieved efficient desorption and made possible the re-use of the sorbent for a minimum of five

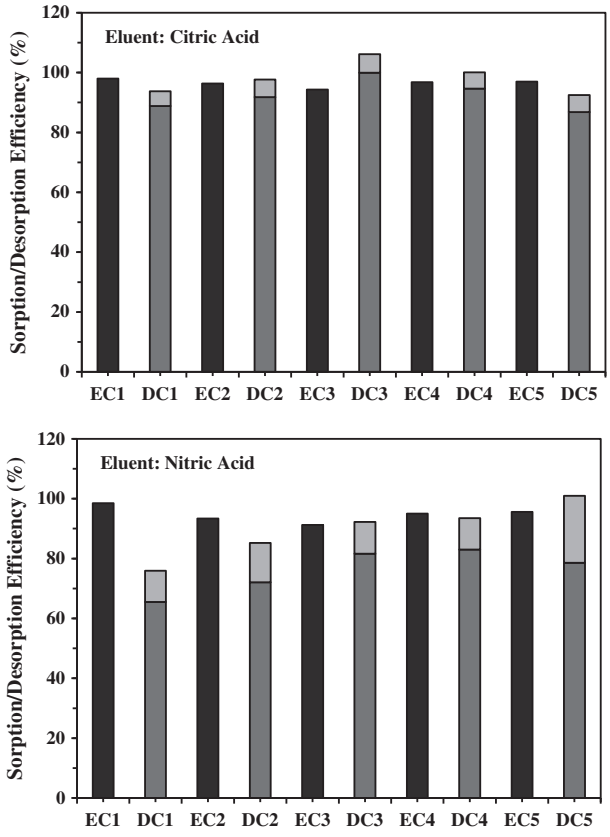

Fig. 10. Sorption (EC)/desorption (DC) cycles using citric acid or nitric acid as eluent (Sorption: C_{HCl}: 1 M; q_{IL}: 401 mg IL g^{-1} EIR; SD: 2 g EIR L^{-1}; C_0: 100 mg Bi L^{-1}; v: 150 rpm; contact time: 24 h/Desorption: two successive treatments with contact time: 24 h; SD: 2 g EIR L^{-1}; [citric acid]: 0.05 M and pH 6; [nitric acid]: 2 M; preconditioning of the resin after desorption: twice with 10 mL of 1 M HCl solution for 2 h).

cycles. These results demonstrate the potential of these materials for Bi(III) recovery from HCl solutions.

4. Conclusions

Cyphos IL101 immobilized on Amberlite XAD-7 can be efficiently used for Bi(III) recovery from HCl solutions (in the range of concentration 0.5–2 M). Sorption efficiency proceeds to chloride ion exchange with Bi(III) chloro-anionic species. The sorption efficiency depends on both HCl concentration and IL loading. Sorption capacity increases with IL loading and the stoichiometric ratio at saturation of the EIR correspond to a molar ratio Bi(III)/IL close to 0.5: this means that $BiCl_5^{2-}$ is the preferential species to be exchanged with chloride ions. The presence of competitor ions, such as Cu(II) and Ni(II) does not interfere on sorption performance since these metals do not form stable chloro-anionic species; on the opposite hand Zn(II) forms stable anionic chloro-complexes and tend to slightly decrease Bi(III) sorption capacities. However, even with a large molar excess the loss of sorption efficiency remains rather limited. The negligible effect of agitation speed on uptake kinetics means that film diffusion is not the main rate limiting step. The good fit of experimental data by the Crank's equation confirms that uptake kinetics are mainly controlled by the resistance to intraparticle diffusion. The diffusion of metal species is hindered (compared to diffusion in water) and the progressive saturation of the porous network induces an increasing resistance to intraparticle diffusion. Increasing the temperature allows limiting this resistance to diffusion, probably due the decrease of IL viscosity. Bi(III) can be readily desorbed from loaded EIR using citric acid solution (0.05 M, pH 6), which is slightly better than 2 M nitric acid solution in terms of Bi(III) sorption and desorption: the performances are maintained at a constant level for a minimum of five sorption/desorption cycles.

Acknowledgments

Authors acknowledge the financial support from the University of Guanajuato (CIAI 2012, 051/12). Cytec (Canada) is acknowledged for the gift of Cyphos IL-101 sample. Authors thank Jean-Marie Taulemesse from C2MA (Ecole des mines d'Alès) for SEM–EDX analysis.

Appendix A. Supplementary material

Supplementary data associated with this article can be found, in the online version, at http://dx.doi.org/10.1016/j.seppur.2014.02.023.

References

[1] P.P. Sheng, T.H. Etsell, Recovery of gold from computer circuit board scrap using aqua regia, Waste Manage. Res. 25 (4) (2007) 380.
[2] W.J. Hall, P.T. Williams, Separation and recovery of materials from scrap printed circuit boards, Resour. Conserv. Recy. 51 (3) (2007) 691.
[3] V. Baboudjian, J. Stafiej, Selective bismuth and antimony removal from copper electrolyte, Hydrometallurgy 46 (3) (1997) 386.
[4] I. Giannopoulou, D. Panias, Copper and nickel recovery from acidic polymetallic aqueous solutions, Miner. Eng. 20 (8) (2007) 753.
[5] T. Hannel, E. Otu, M. Jensen, Thermochemistry of the extraction of bismuth(III) with bis(2-ethylhexyl) phosphoric and 2-ethyhexyl-phenylphosphonic acids, Solvent Extr. Ion Exch. 25 (2) (2007) 241.
[6] S.G. Sarkar, P.M. Dhadke, Solvent extraction separation of antimony(III) and bismuth(III) with bis(2,4,4-trimethylpentyl) monothiophosphinic acid (Cyanex 302), Sep. Purif. Technol. 15 (2) (1999) 131.
[7] J.A. Reyes-Aguilera, M.P. Gonzalez, R. Navarro, T.I. Saucedo, M. Avila-Rodriguez, Supported liquid membranes (SLM) for recovery of bismuth from aqueous solutions, J. Membr. Sci. 310 (1–2) (2008) 13.
[8] R. Wang, X.-P. Liao, S.-L. Zhao, B. Shi, Adsorption of bismuth(III) by bayberry tannin immobilized on collagen fiber, J. Chem. Technol. Biotechnol. 81 (7) (2006) 1301.
[9] K. Oshita, O. Noguchi, M. Oshima, S. Motomizu, Synthesis of cross-linked chitosan modified with the glycine moiety for the collection/concentration of bismuth in aquatic samples for ICP-MS determination, Anal. Sci. 23 (10) (2007) 1203.
[10] V. Dedkova, O. Shvoeva, S. Savvin, Adsorption and determination of bismuth with 4-(2-pyridylazo)resorcinol on a fibrous ion exchanger, J. Anal. Chem. 65 (6) (2010) 577.
[11] M.S. El-Shahawi, A. Hamza, A.A. Al-Sibaai, H.M. Al-Saidi, Fast and selective removal of trace concentrations of bismuth (III) from water onto procaine hydrochloride loaded polyurethane foams sorbent: Kinetics and thermodynamics of bismuth (III) study, Chem. Eng. J. 173 (1) (2011) 29.
[12] B. Mandal, N. Ghosh, Combined cation-exchange and extraction chromatographic method of preconcentration and concomitant separation of bismuth(III) with high molecular mass liquid cation exchanger, J. Hazard. Mater. 182 (1–3) (2010) 363.
[13] E.A. Moawed, A.B. Farag, M.F. El-Shahat, Separation and determination of some trivalent metal ions using rhodamine B grafted polyurethane foam, J. Saudi Chem. Soc. 17 (1) (2013) 47.
[14] N. Tokman, S. Akman, M. Ozcan, Solid-phase extraction of bismuth, lead and nickel from seawater using silica gel modified with 3-aminopropyltriethoxysilane filled in a syringe prior to their determination by graphite furnace atomic absorption spectrometry, Talanta 59 (1) (2003) 201.
[15] N.-E. Belkhouche, M.A. Didi, Extraction of Bi(III) from nitrate medium by D2EHPA impregnated onto Amberlite XAD-1180, Hydrometallurgy 103 (1–4) (2010) 60.
[16] M. Blahušiak, Š. Schlosser, J. Marták, Extraction of butyric acid by a solvent impregnated resin containing ionic liquid, React. Funct. Polym. 71 (7) (2011) 736.
[17] A. Cieszynska, M. Wiśniewski, Extractive recovery of palladium(II) from hydrochloric acid solutions with Cyphos®IL 104, Hydrometallurgy 113–114 (2012) 79.
[18] M.L. Dietz, Ionic liquids as extraction solvents: where do we stand?, Sep Sci. Technol. 41 (10) (2006) 2047.
[19] L. Fischer, T. Falta, G. Koellensperger, A. Stojanovic, D. Kogelnig, M. Galanski, R. Krachler, B.K. Keppler, S. Hann, Ionic liquids for extraction of metals and metal

containing compounds from communal and industrial waste water, Water. Res. 45 (15) (2011) 4601.
[20] M. Regel-Rosocka, M. Wisniewski, Selective removal of zinc(II) from spent pickling solutions in the presence of iron ions with phosphonium ionic liquid Cyphos IL 101, Hydrometallurgy 110 (1–4) (2011) 85.
[21] S. Wellens, B. Thijs, K. Binnemans, An environmentally friendlier approach to hydrometallurgy: highly selective separation of cobalt from nickel by solvent extraction with undiluted phosphonium ionic liquids, Green Chem. 14 (6) (2012) 1657.
[22] Y. Liu, L. Guo, L. Zhu, X. Sun, J. Chen, Removal of Cr(III, VI) by quaternary ammonium and quaternary phosphonium ionic liquids functionalized silica materials, Chem. Eng. J. 158 (2) (2010) 108.
[23] D. Shanthana Lakshmi, A. Figoli, G. Fiorani, M. Carraro, L. Giorno, E. Drioli, Preparation and characterization of ionic liquid polymer microspheres [PEEKWC/DMF/CYPHOS IL 101] using the phase-inversion technique, Sep. Purif. Technol. 97 (2012) 179.
[24] A. Arias, I. Saucedo, R. Navarro, V. Gallardo, M. Martinez, E. Guibal, Cadmium(II) recovery from hydrochloric acid solutions using Amberlite XAD-7 impregnated with a tetraalkylphosphonium ionic liquid, React. Funct. Polym. 71 (11) (2011) 1059.
[25] R. Navarro, I. Saucedo, C. Gonzalez, E. Guibal, Amberlite XAD-7 impregnated with cyphos IL-101 (tetraalkylphosphonium ionic liquid) for Pd(II) recovery from HCl solutions, Chem. Eng. J. 185–186 (2012) 226.
[26] R. Navarro, I. Saucedo, A. Nunez, M. Avila, E. Guibal, Cadmium extraction from hydrochloric acid solutions using Amberlite XAD-7 impregnated with Cyanex 921 (tri-octyl phosphine oxide), React. Funct. Polym. 68 (2) (2008) 557.
[27] K. Campos, R. Domingo, T. Vincent, M. Ruiz, A.M. Sastre, E. Guibal, Bismuth recovery from acidic solutions using Cyphos IL-101 immobilized in a composite biopolymer matrix, Water. Res. 42 (14) (2008) 4019.
[28] E. Guibal, T. Vincent, C. Jouannin, Immobilization of extractants in biopolymer capsules for the synthesis of new resins: a focus on the encapsulation of tetraalkylphosphonium ionic liquids, J. Mater. Chem. 19 (45) (2009) 8515.
[29] T. Vincent, A. Parodi, E. Guibal, Pt recovery using Cyphos IL-101 immobilized in biopolymer capsules, Sep. Purif. Technol. 62 (2) (2008) 470.
[30] V. Gallardo, R. Navarro, I. Saucedo, M. Avila, E. Guibal, Zinc(II) extraction from hydrochloric acid solutions using Amberlite XAD-7 impregnated with Cyphos IL 101 (tetradecyl(trihexyl)phosphonium chloride), Sep. Sci. Technol. 43 (9–10) (2008) 2434.
[31] R.-S. Juang, Preparation, properties and sorption behavior of impregnated resins containing acidic organophosphorus extractants, Proc. Natl. Sci. Counc. ROC(A) 23(3) (1999) 353.
[32] L. Hinojosa Reyes, T.I. Saucedo Medina, R. Navarro Mendoza, J. Revilla Vasquez, M. Avila Rodriguez, E. Guibal, Extraction of cadmium from phosphoric acid using resins impregnated with organophosphorus extractants, Ind. Eng. Chem. Res. 40 (5) (2001) 1422.
[33] R. Navarro, I. Saucedo, M.A. Lira, E. Guibal, Gold(III) recovery from HCl solutions using Amberlite XAD-7 impregnated with an ionic liquid (Cyphos IL-101), Sep. Sci. Technol. 45 (12–13) (2010) 1950.
[34] E. Högfeldt, Stability Constants of Metal-Ion Complexes. Part A: Inorganic Ligands, first ed., Reprinted 1983, Pergamon Press, Great Britain, 1982.
[35] K. Campos, T. Vincent, P. Bunio, A. Trochimczuk, E. Guibal, Gold recovery from HCl solutions using Cyphos IL-101 (a quaternary phosphonium ionic liquid) immobilized in biopolymer capsules, Solvent Extr. Ion Exch. 26 (5) (2008) 570.
[36] M. Avila Rodriguez, D.F. Cholico, M.P. Gonzalez, R. Navarro, T.I. Saucedo, Recovery of Fe(III) from acidic solutions by SLM using Cyphos IL 101 ionic liquid as carrier, in: S.V. Gorley (Eds.), Handbook in Membrane Research: Properties, Performance and Applications", Nova Science Publishers, New York, USA, 2009, pp. 465–482.
[37] A. Sartape, A. Mandhare, P. Salvi, D. Pawar, P. Raut, M. Anuse, S. Kolekar, Removal of Bi (III) with adsorption technique using coconut shell activated carbon, Chin. J. Chem. Eng. 20 (4) (2012) 768.
[38] M. Regel-Rosocka, Extractive removal of zinc(II) from chloride liquors with phosphonium ionic liquids/toluene mixtures as novel extractants, Sep. Purif. Technol. 66 (1) (2009) 19.
[39] M. Regel-Rosocka, L. Nowak, M. Wisniewski, Removal of zinc(II) and iron ions from chloride solutions with phosphonium ionic liquids, Sep. Purif. Technol. 97 (2012) 158.
[40] T. Vincent, A. Parodi, E. Guibal, Immobilization of Cyphos IL-101 in biopolymer capsules for the synthesis of Pd sorbents, React. Funct. Polym. 68 (7) (2008) 1159.
[41] F.J. Alguacil, M. Alonso, F.A. Lopez, A. Lopez-Delgado, Pseudo-emulsion membrane strip dispersion (PEMSD) pertraction of chromium(VI) using CYPHOS IL101 ionic liquid as carrier, Environ. Sci. Technol. 44 (19) (2010) 7504.